Assessment of in-situ stress distribution and mechanical properties of wooden foundation piles instrumented with distributed fiber optic sensors (DFOS)

Felicita, Maria; Pagella, Giorgio; Ravenshorst, Geert; Mirra, Michele; van de Kuilen, Jan Willem

DOI
10.1016/j.cscm.2024.e03139

Publication date
2024

Document Version
Final published version

Published in
Case Studies in Construction Materials

Citation (APA)
Felicita, M., Pagella, G., Ravenshorst, G., Mirra, M., & van de Kuilen, J. W. (2024). Assessment of in-situ stress distribution and mechanical properties of wooden foundation piles instrumented with distributed fiber optic sensors (DFOS). *Case Studies in Construction Materials*, *20*, Article e03139. https://doi.org/10.1016/j.cscm.2024.e03139

Case Studies in Construction Materials 20 (2024) e03139

Contents lists available at ScienceDirect

Case Studies in Construction Materials

journal homepage: www.elsevier.com/locate/cscm

Assessment of in-situ stress distribution and mechanical properties of wooden foundation piles instrumented with distributed fiber optic sensors (DFOS)

Maria Felicita [a,1], Giorgio Pagella [a,*,2], Geert Ravenshorst [a,3], Michele Mirra [a,4], Jan-Willem van de Kuilen [a,b,5]

[a] Delft University of Technology, Faculty of Civil Engineering and Geosciences, Biobased Structures and Materials, Delft 2628CN, the Netherlands
[b] Technical University of Munich, School of Engineering and Design, Wood Technology, München 80333, Germany

ARTICLE INFO

Keywords:
Wooden foundation piles
Distributed fibre optic sensors (DFOS)
In-situ stress assessment
DFOS validation
Mechanical properties
Assessment and monitoring

ABSTRACT

This case study explores the utilization of distributed fiber optic sensors (DFOS) in wooden foundation piles, for assessing and monitoring the stress distribution along their length. Three spruce and three pine foundation piles instrumented with DFOS were driven into the soil in a testing field in Amsterdam and axially loaded in compression. Since DFOS provided strain information, calculating the stress distribution in the piles required knowledge of their stiffness properties, which inherently vary from the head to the tip. Consequently, the piles were extracted and their overall wet dynamic elastic modulus ($E_{c,0,dyn,wet}$) was determined through frequency response measurements. Subsequently, the piles were segmented, transported to the TU Delft Laboratory and subjected to mechanical testing. For each segment, the mechanical properties were determined and their variability along the pile was studied, in particular for the static modulus of elasticity ($E_{c,0,stat,wet}$). This enabled a comprehensive assessment of the actual in-situ stress distribution ($\Delta\sigma_{actual,stat}$ and $\Delta\sigma_{actual,dyn}$) along the length of the piles, calculated with DFOS strains and the pile stiffness ($E_{c,0,stat,wet}$ and $E_{c,0,stat,dyn}$). Given the novelty of the DFOS application to timber piles, a validation of the accuracy was conducted on 3 pile segments equipped with DFOS. These segments underwent laboratory compression testing, allowing for a direct comparison between DFOS strain readings and strains measured with linear potentiometers attached to the pile segments. The results revealed good accuracy of DFOS in controlled lab conditions, with a maximum stress deviation of 0.65 MPa. Since the testing field featured a 6-meter-deep predrilled layer, where negligible shaft friction was mobilized, the no-friction stress ($\Delta\sigma_{no\text{-}friction}$) approximately aligned with $\Delta\sigma_{actual,stat}$ on the piles. At pile tips, the maximum applied 300–350 kN compressive load (i.e. $\Delta\sigma_{no\text{-}friction}$ = 20–26 MPa), resulted in $\Delta\sigma_{actual,stat}$ = 4–7 MPa, highlighting shaft friction effect. The calculated $\Delta\sigma_{actual,dyn}$ with a single $E_{c,0,stat,dyn}$ for the whole pile, led to 3 MPa stress overestimation at pile tip. Although this calculation is conservative, the

* Corresponding author.
E-mail address: g.pagella@tudelft.nl (G. Pagella).
[1] 0000000329786724
[2] 0000-0002-2552-4877
[3] 0000-0002-1462-5584
[4] 0000-0002-9898-8971
[5] 0000-0001-6974-3783

https://doi.org/10.1016/j.cscm.2024.e03139
Received 4 December 2023; Received in revised form 14 March 2024; Accepted 6 April 2024
Available online 8 April 2024

detailed knowledge of the variation of stiffness properties along the pile would result in a more efficient structural use.

1. Introduction

1.1. Timber foundation piles and design code

In the city of Amsterdam, a large number of existing structures rely on the load-carrying capacity of thousands of spruce (*Picea abies*) and pine (*Pinus sylvestris*) foundation piles, due to the presence of weak soils, mainly composed of clay and peat layers up to approximately 12 m depth [1]. Over the years, timber foundations in Amsterdam have proven to be a cost-efficient solution achieving adequate performance [2,3]. Presently, the evaluation of the current condition and remaining load-carrying capacity of timber foundation piles has become crucial, given the phenomena of biodegradation of timber and the aging of foundations, some of which may be up to 500 years old [4–8]. Even in cases where the wooden foundations are in satisfactory condition, a structural assessment is often needed when modification, maintenance or renovation works of existing structures are planned. However, conducting a proper engineering assessment on the behaviour of (existing) timber foundation piles is difficult, since in the current Eurocode 5 (EC5) EN 1995–1–1 [9], that provides regulations for the design of timber structures, timber foundation piles are not mentioned. This limits the ability to conduct a comprehensive engineering assessment of timber foundations within the European context. In the Netherlands, the current National Annex to EC5, NEN-EN 1995–1-1/NB:2013 [10] and NEN 5491 Timber Piles (2010) [11], provide design values and grading rules for timber foundation piles and their application in the soil. In the previous Dutch National Annex to EC5, NEN-EN 1995–1–1/NB:2007 [12], one strength value for the dry compressive strength $f_{c,0,k} = 19.8\,N/mm^2$ at 12 % moisture content was provided for timber piles. In order to account for long-term loading and the effect of high moisture content, a design wet compressive strength value $f_{c,0,d} = 9.8\,MPa$ is reported in [10], assuming that wooden piles are completely submerged under the water table. However, no design values for the modulus of elasticity parallel to the grain are reported. Moreover, the values given in [10] and [12] do not account for the variability in strength and stiffness within the tapered pile, both longitudinally along its length and transversely across its cross-section. This limitation hinders a comprehensive analysis of the load-bearing capacity in relation to the stresses acting along a timber pile subjected to axial loads. It is important to underscore that the stiffness and compressive strength of softwoods, such as spruce and pine, increases from the top log to the butt log, in relation to the increasing wood density due to larger diameters, bigger proportion of mature wood, larger latewood content and smaller annual ring width [13–16]. In this context, the mechanical characterization of saturated timber foundation piles is needed for an adequate assessment, as reported in the new draft of the Annex to EC5, prEN 1955–1–1/NB:2023 [17], where characteristic values for wet compressive strength and stiffness in saturated conditions shall be derived with mechanical testing.

1.2. In-situ stress distribution

The stress distribution acting along an axially loaded pile is influenced by both the stiffness distribution along the pile length and the shaft friction between the pile and the soil. According to NEN 9997–1 [18], the part of the axial load carried through the shaft friction of the pile can be estimated based on the resistance characteristics of the different soil layers and the geometrical properties of the pile. The remaining component of the axial load must be taken all the way to the pile tip, which will transfer it to the load carrying soil layer. It is important to assess that the stress level along the pile does not reach the strength capacity, in order to avoid the compressive failure of the pile.

The stress level ($\sigma = E \bullet \varepsilon$) over a given element can be estimated based on the strain deformations (ε) and stiffness (E). For timber foundation piles, the estimation of both components can be challenging, since in the current standards no stiffness values parallel to the grain are provided. As explained in Section 1.1, the stiffness properties can vary along the length of the pile, due to its tapered nature and the changing ratio of juvenile and mature wood [13–16]. Moreover, the assessment of the strain deformations along timber foundation piles becomes challenging once the piles are driven in-situ, due to limited access. Common practice is to measure the head displacement of an axially loaded pile with respect to the soil level [19]. However, this method does not provide information about the strain distribution along the length, which is essential for determining the in-situ stresses in the pile.

In order to assess the strain distribution along the pile, Distributed Fiber Optic Sensors (DFOS) can be used. DFOSs are an emerging technology in the field of civil engineering, which proved to be reliable when employed in monitoring the strains of in-situ cast reinforced concrete piles subjected to axial loads [20,21]. However, the use of DFOS in timber foundation piles is novel and limited in literature. In contrast to concrete piles, which maintain a uniform and constant cross-section throughout their length, and whose material is regarded as homogeneous for engineering calculations [22], the utilization of DFOS on timber piles addresses the challenges posed by the heterogeneity of the material, the variability in stiffness properties along the pile and the tapered shape. To this end, the validation of DFOS application is conducted with a specific focus on its suitability in strain measurements for timber piles (Section 3.3).

1.3. Case study and research objective

The case study presented in this article comprised 3 spruce (*Picea abies)* piles from the Netherlands and 3 pine (*Pinus sylvestris*) piles

from Germany, that were equipped with distributed fiber optic sensors (DFOS) and driven into the ground in a test field located in the Overamstel area (Amsterdam, NL). The in-situ driving of the piles was part of a large geotechnical program conducted by the Municipality of Amsterdam (*Toetsingskader Amsterdamse Bruggen*, TAB). The full-length piles were preloaded in-situ to geotechnical failure, correspondent to a maximum displacement of the head of the pile equal to 10 % of the head diameter, in accordance with NEN 9997–1+C2:2017 [18]. The short-term loading tested were conducted within a day, with maximum stress level of 8.1 MPa measured on the pile head. During the load application, the DFOSs collected the corresponding distributed strain measurements. The investigation aimed to measure the in-situ stress distribution along the length of the axially loaded piles equipped with DFOS. The accuracy of the DFOS measurements was studied taking into account the variability of the mechanical properties along timber piles, on the basis of the following investigations:

- Strain measurements can only be related to the acting stress by knowing the wet stiffness variation ($E_{c,0,stat,wet}$) along the tapered pile. Therefore, after in-situ testing, the timber piles were extracted, subdivided in ca. 8 segments and subjected to mechanical testing in order to characterize the distribution of mechanical properties along each pile (Section 3.2). The in-situ stress distribution was calculated by considering the varying distribution of $E_{c,0,stat,wet}$ along the pile, based on the stiffness of each tested pile segment, and a single dynamic modulus of elasticity $E_{c,0,dyn,wet}$ derived for the whole pile with frequency response measurements (Section 3.2).
- DFOSs are a novel technology for assessing the strain distribution of timber piles. A validation of the DFOS application was carried out in order to reliably interpret the in-situ DFOS strain measurements (Section 3.3). To this end, the last 4-m-tip of the piles, equipped with DFOS used in-situ, were tested in the laboratory under compressive loads. During the application of axial loading, the strains were measured with both DFOS and linear potentiometers (LP) to validate the strain readings (Section 3.3).

For better clarity, Fig. 1 shows the workflow used to collect the data studied within this paper.

2. Materials

In this research work, six timber piles were investigated:

– 3 spruce (*Picea abies*) piles felled in a forest in Holterberg, The Netherlands.
– 3 pine (*Pinus sylvestris*) piles felled in a forest in Nuremberg, Germany.

The piles were felled in the year 2019, debarked, and had an average length of 13.6 m, an average head diameter of 240 mm and average tip diameter of 140 mm. After the in-situ loading, the six piles were extracted and subdivided in three parts: heads (ca. 4 m), middle-parts (ca. 4 m) and tips (ca. 6 m). After the DFOS validation (Section 3.3), heads, middle-parts and tips were further subdivided in 47 segments (Section 3.2).

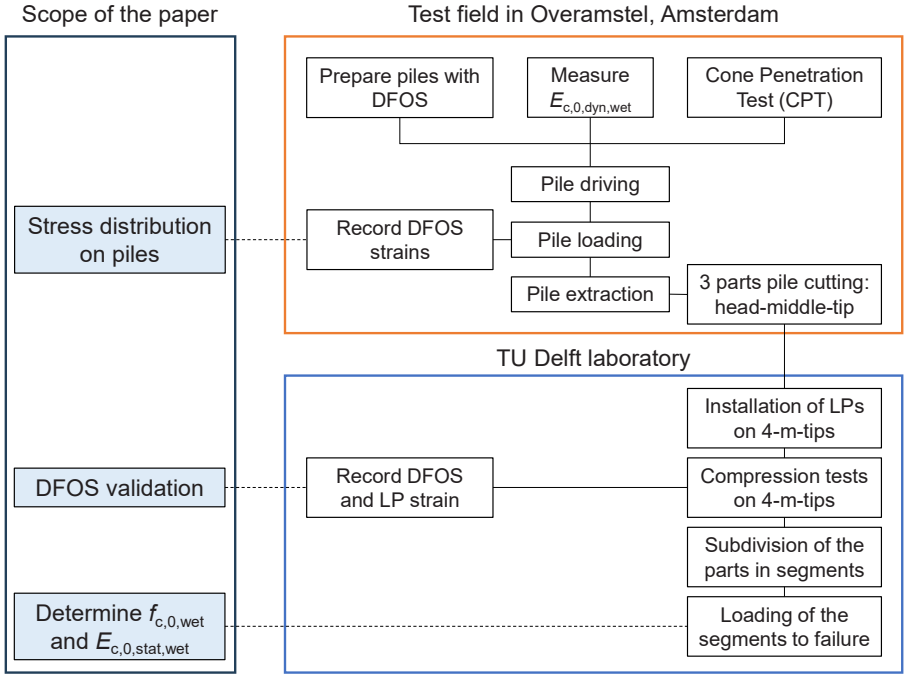

Fig. 1. Workflow of the research study presented in the article.

3. Methods

3.1. In-situ testing

As part of the experimental framework *Toetsingskader Amsterdamse Bruggen* (TAB), a total of 6 wooden piles were driven into the soil in a testing site in Overamstel, Amsterdam (NL). Each pile was instrumented with DFOSs. The DFOS consisted of two optical fiber cables *G657A (Single mode),* inserted in a polyethylene cable with two metal strands reinforcing on each side of the optical fiber [23]. Two cables were glued inside an incision along the length of the pile on four sides (Fig. 2b). The piles were instrumented in quadrants, i.e. two loops of DFOSs were installed on four sides of each pile. Two cables were used: every cable covered two sides, starting from the pile head, to the pile tip and coming back to the head. Two channels were adopted, labelled North-South and East-West (Fig. 2a). Approximately 30 cm from the pile tip, the wood was drilled to loop the fibers within the pile. This was done to have an uninterrupted cable installed on two sides of the pile. The procedure is illustrated in Fig. 2a, where the pile section was first drilled, to pass the fibers through the pile core, and finally the fibers were kept in position by using 3D-printed filling pieces (Fig. 2c). During the axial loading of the pile, the DFOSs measured strains simultaneously. The spatial resolution of each fiber optic sensor was 250 mm.

Two Cone Penetration Tests (CPTs) were conducted at each pile location to get a comprehensive understanding of the soil profile and cone resistance at the site. A static load frame was installed on top of the piles (Fig. 3a), with the purpose of imposing short-term compression loads with increasing load steps. The pile head was approximately 1.5 m above the ground level, and on top of it, a load cell and two displacement sensors (Linear Variable Differential Transducers or LVDTs) were placed to measure the push-out of the load cell (Fig. 3b).

3.1.1. Data collection

All the 6 piles were subjected to short-term loading according to Table 1, which lists the highest load step (ΔF) and the number of load steps (different for every pile). The highest load step corresponded to the geotechnical failure, i.e. 10 % of the head diameter ($0.1D_{head}$), in accordance with NEN 9997–1+C2:2017 [18]. The pile head was always 1.5–2 m above the water level: in this part of the pile, the strains were not measured with DFOS. The load cell and displacement sensors automatically recorded the applied load and head displacement every second.

The DFOS were connected to an Omnisens interrogator [24] to interpret the strain measurements. The interpreter collects the data based on the photonic principle which measures changes in the molecular structure of the glass along the fibre [25]. During this test, the strain measurements were manually recorded approximately every 5 minutes for each DFOS channel. The Municipality of Rotterdam was in charge of the DFOS strain data collection.

3.1.2. Data processing

The strain measurements acting over a given pile cross section can be converted into a stress level by relating them to the modulus of elasticity at the given cross section. Because the DFOSs were already installed in the pile during the driving process, there might be an existing strain on the readings, not related to the applied axial load. Thus, to investigate the actual stress acting on the pile as a result of an applied load, the relative change in strain $\Delta\varepsilon_{DFOS}$ over different load levels was considered. The actual stress $\Delta\sigma_{actual,stat}$ acting on the pile was determined using Eq. 1, where $E_{c,0,stat,wet}$ is the wet static modulus of elasticity, determined for individual saturated pile segments as described in Section 3.2.

$$\Delta\sigma_{actual,stat} = E_{c,0,stat,wet} * \Delta\varepsilon_{\mathrm{DFOS}} \tag{1}$$

Additionally, to visualize the effect of considering the distributed stiffness properties of the pile on the stress distribution, the overall stress acting on the pile $\Delta\sigma_{actual,dyn}$ was also determined using Eq. 2, where $E_{c,0,dyn,wet}$ is the wet dynamic modulus of elasticity,

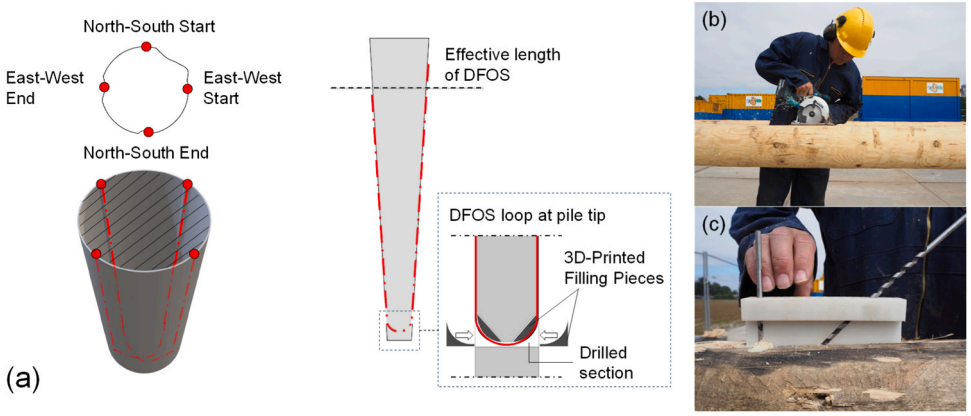

Fig. 2. (a) Position and layout of DFOSs along a timber pile and detail of fiber loop in the pile tip; (b) grooves drilling for DFOS installation; (c) 3D-printed plastic-filling piece to keep the fiber loop in position at the pile tip.

Fig. 3. (a) In-situ loading set-up applied to a wooden foundation pile in Overamstel (Amsterdam, NL); (b) LVDTs applied to the pile head to monitor the displacement during loading.

Table 1
Number of load steps, highest load step, and pile head location of the 6 piles in-situ loaded in Overamstel.

Pile ID	Species	No. load steps	Highest load step ΔF (kN)	Pile head above NAP[a] (m)
164	Spruce	6	350	1.9
398	Spruce	9	325	1.5
397	Spruce	9	375	2.2
592	Pine	7	375	1.5
576	Pine	5	300	1.5
594	Pine	8	325	1.4

[a] NAP: *Nieuw Amsterdams Peil* - reference plane for water table (North Sea level)

determined for the full pile as described in Section 3.2.

$$\Delta\sigma_{actual,dyn} = E_{c,0,dyn,wet} * \Delta\varepsilon_{\mathrm{DFOS}} \tag{2}$$

The no-friction stress acting over a given pile cross section is referred to as the stress that would be expected without any friction between the pile and the soil. The no-friction stress $\Delta\sigma_{no\text{-}friction}$ at a given change in load level can be determined with Eq. 3, where $A_{applied}$ is the given cross-section of interest.

$$\Delta\sigma_{no-friction} = \frac{\Delta F_{applied}}{A_{applied}} \tag{3}$$

3.1.3. Data analysis

In order to visualize the effect of the soil and the load acting along the length of the pile, the actual stress was compared to the no-friction stress at a specific load change, under the assumption that without soil interaction these two should be equal along the length of the pile. The load level has an effect on the load distribution, thus the actual stress acting on the pile at different load levels was studied. Temperature-induced strain alterations were not measured during in-situ pile testing with DFOS, primarily due to the limited time span of each loading test, which lasted approximately 2 hours. The initial strains after pile installation and before the in-situ test, corresponded to a maximum of 100 με at the pile base and 120 με in the clay layer. These strains were zeroed in the post-processing of the strain measurements. The initial strains could be attributed to many factors: (a) the recovery of shear surfaces by the surrounding soil as a time dependent effect; (b) potential surface settlement; (c) dissipation of pore pressures after the installation of the pile; (d) alterations in moisture content and changes in temperature (not measured); (e) geometrical variability along the pile; (f) consolidation of the disturbed soil. Each of these factors could have caused the initial micro strains, but it was not possible to quantify their individual contribution. In terms of stress on the pile, the initial strain would result on average into a stress increase of 0.5 MPa in the tips and 0.7 MPa in the middle-part of the pile, with an influence of about 10 % on the maximum stress reached during the in-situ compression loading of the piles. Consequently, the potential impact of the aforementioned factors were neglected in the data analysis, focusing only on the stresses along the piles induced by the applied in-situ loading.

3.2. Mechanical testing of pile segments

In spring 2021, the timber piles were extracted from the test field without removing the DFOSs and tested over the whole length

with frequency response measurements, to determine the dynamic modulus of elasticity ($E_{c,0,dyn,wet}$). Subsequently, the piles were cut in smaller segments, representative for head (K), middle-part (M) and tip (V), from the Dutch words *kop, middenstuk* and *voet,* respectively; in this phase, the DFOSs were kept only into the pile tips. The adopted labelling system is shown in Table 2. The pile parts were submerged under water in containers, to recreate the same in-soil conditions where the piles were fully under the water table, in order to retrieve comparable mechanical and physical properties during testing. The containers were transported to the TU Delft Stevin II laboratory. At the arrival, the pile tips were cut at the bottom in order to obtain a 4- m segment equipped with DFOSs. Every segment was tested in compression to validate the strains of DFOS with the strain obtained from the linear potentiometers attached to the specimens (Section 3.3.2). Each main part was further cut in different segments (Fig. 4), leading to the following final coding scheme, taking as an example pile 398 (OAM-P1.1):

- Head: K1.1 K - K1.1 M - K1.1 V
- Middle: M1.1 K - M1.1 M - M1.1 V
- Tip: V1.1 K - V1.1 V

After the test of the 4-m tip (V…V) for DFOS validation, this part was subsequently divided in 3 segments, respectively coded as V1.1Vc, V1.1Vb and V1.1Va, for a more accurate investigation of the mechanical properties along the tip. The labelling and cutting position of the segments is represented in Fig. 4.

The subdivision in smaller segments allowed to determine the axial wet compressive strength and static modulus of elasticity parallel to the grain, as well as their variation along the piles. Each segment had a length of approximately 6 times the smallest diameter of the conical log sections according to EN 408 [28]. This was done to investigate the strength and stiffness profile over the length of the tapered piles, with a consistent slenderness ratio of 1:6 in accordance with the testing procedures outlined in EN 408. Before testing and between handling procedures, the segments were constantly kept under water, aiming for a moisture content higher than 70 %, to recreate in-soil conditions.

The compression tests were carried out on a displacement-controlled set-up where the wooden piles were placed between two parallel steel plates. Before running full-scale mechanical testing on the pile segments, the specimens were taken out of the water, and the density of each pile was measured by determining volume and wet mass (EN 384 [26]). The moisture content was calculated with input values of dry and wet mass of each pile segment in accordance with EN 13183 [27]. Therefore, any variation of the wet mass of the pile could be related to a precise moisture content value. Mechanical testing was performed to determine the wet compressive strength ($f_{c,0,wet}$) and static modulus of elasticity ($E_{c,0,stat,wet}$) parallel to the grain. From the original 6 piles, the mechanical properties of a total of 47 pile segments were determined. To this end, a displacement-controlled set-up was used (Fig. 5), based on standards EN 408 [28] and EN 14251 [29], where the specimens were subjected to an axial load in direction parallel to the grain. The displacement between the two steel plates was monitored with four linear potentiometers (S1-S4 in Fig. 5) placed on four edges of the top plate and connected to the bottom plate. The deformation of the specimens was measured with four linear potentiometers (P1-P4 in Fig. 5) that were attached to the surface of the pile, positioned at 90° intervals on each side of the sample, with a variable length equal to two-thirds of its length. Given the short stroke (± 20 mm) of the four P-sensors placed on the pile, they were removed right after the peak load to avoid damages. The post-peak softening was monitored only by the S-potentiometers attached to the top and bottom steel plates of the compression machine. In addition, a hinge, mounted on a steel plate, was placed on top of the specimen to guarantee an uniformly distributed compression load on the pile.

The compression test was carried out at a constant displacement of 0.02 mm/s. The maximum load was reached within 5 ± 2 minutes for every samples, according to EN 408. After the peak load, the test continued at a higher speed to record the post-peak behaviour of the pile until the cracks were visible.

Upon completion of the test, $f_{c,0,wet}$ was calculated by taking the ratio of the maximum force achieved in compression by the specimen and the average cross-sectional area of the pile. The global behaviour of the piles was studied with the average stress-strain curve of the four linear potentiometers connected to the compression test machine (Fig. 6a); the strains were calculated considering the length of the specimen. $E_{c,0,stat,wet}$ was calculated with the stress variation ($\Delta\sigma$) divided by the strain variation ($\Delta\varepsilon$), between 10 % and 40 % in the slope of the linear elastic portion of the stress-strain curve (Fig. 6b). In addition, the wet dynamic modulus of elasticity ($E_{c,0,dyn,wet}$) was determined through the frequency response method [30]. This measurement was performed on every segment prior to testing.

Table 2
Coding and wood species of the six investigated timber piles.

Pile ID	TUD coding	species	Head (K)	Middle-part (M)	Tip (V)
164	OAM-P2.1	Spruce	P2.1 K	P2.1 M	P2.1 V
398	OAM-P1.1	Spruce	P1.1 K	P1.1 M	P1.1 V
397	OAM-P1.4	Spruce	P1.4 K	P1.4 M	P1.4 V
592	OAM-P2.9	Pine	P2.9 K	P2.9 M	P2.9 V
576	OAM-P2.10	Pine	P2.10 K	P2.10 M	P2.10 V
594	OAM-P2.8	Pine	P2.8 K	P2.8 M	P2.8 V

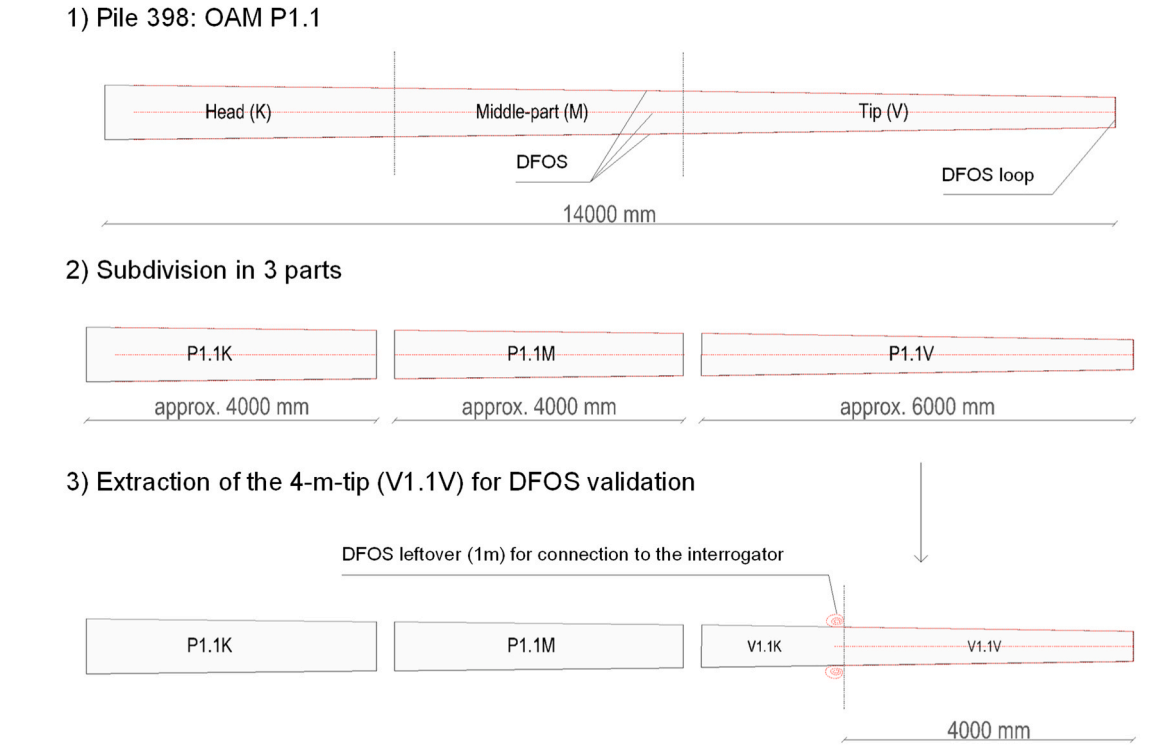

Fig. 4. Example of labelling and subdivision in segments for pile 398-OAM P1.1.

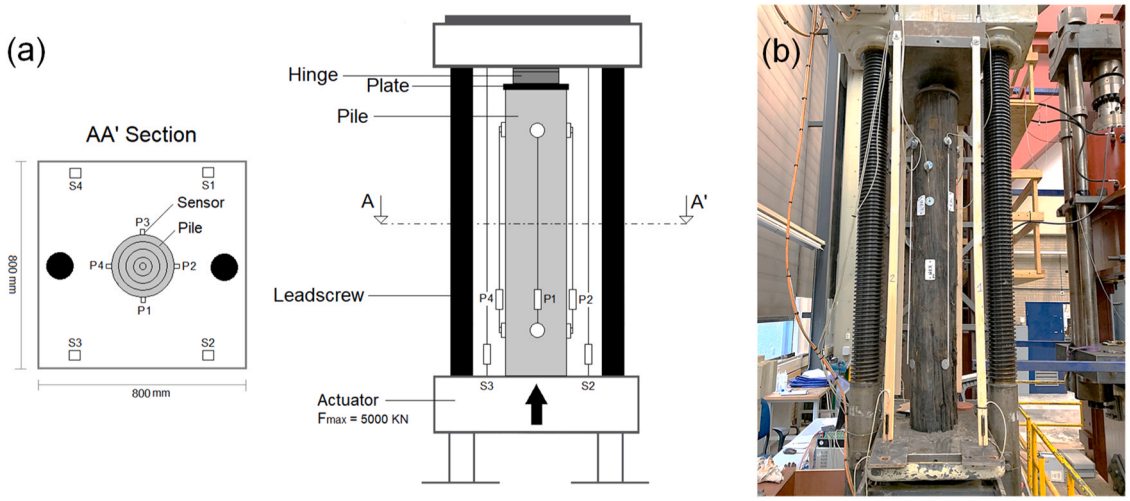

Fig. 5. (a) Set-up for large-scale axial compression test of pile segments; (b) Example of compression test of a pile.

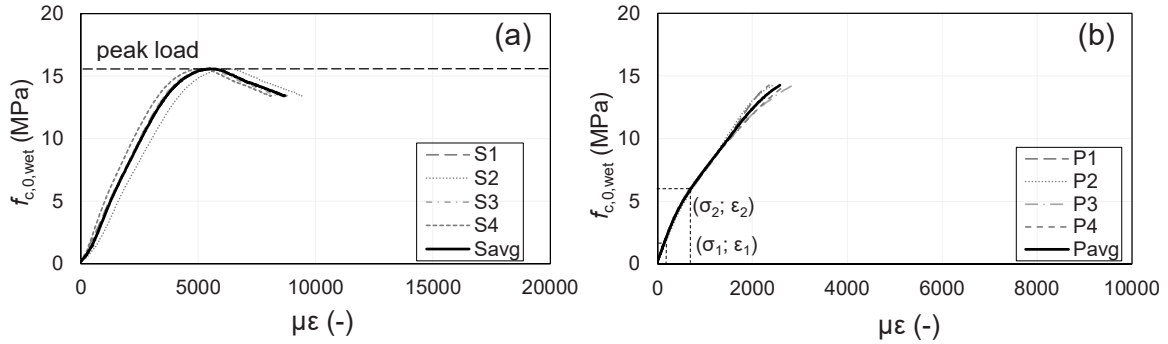

Fig. 6. Example of axial compression tests of pile segment M1.1 V in order to show: (a) global behaviour of the pile, stress-strain curves measured by S1, S2, S3, S4; (b) stress-strain curves measured by P1, P2, P3, P4 to determine $E_{c,0,stat,wet}$.

3.3. Mechanical testing of pile tips for DFOS validation

The validation of the DFOS measurements was carried out by comparing the DFOS strain levels with the strain recordings of additional linear potentiometers attached to the specimens. The pile tips (segments V_V, see Section 3.2) were selected for the validation study based on the location of the fiber loop (Fig. 7): in order to have a comprehensive understanding of the pile behaviour, it is important to collect strain measurements from at least two opposite sides of the pile. During the subdivision in segments, the fibres were also cut. Since the Omnisens interrogator is able to interpret the strain measurements of one DFOS channel at a time, only pile tip segments could provide strain readings over two sides of the sample. The pile tip segments, which were originally ca. 6 m long, were cut into 4-m segments at the opposite side of the loop, by first extracting the DFOS at the top 2 m and then performing the cut in order allow for extra cable length, which was used to connect the DFOS to the interrogator (Fig. 8). It is important to note that out of the 6 piles, only 3 were used for the validation of the method. More specifically, pile 576 (pine), 398 (spruce) and 594 (pine). This was because of the damage in the optical sensors possibly caused by the driving, loading, extraction and cutting of the piles. The softwood species of the 3 selected piles did not influence the DFOS validation, since the distribution of the material properties along the piles, reported in Paragraph 4.2, were comparable for both pine and spruce.

3.3.1. DFOS data collection

The pile tip segments were tested under compression on a load-controlled set-up. For the test, each segment was equipped with 12 linear potentiometers (LPs), attached magnetically on metal plates screwed on the surface of the pile. Three LPs (1 m long) were placed in sequence on each side of the pile, 90 degrees from each other, following the line of the DFOS in the specimen (Fig. 8). Additionally, a hinge was placed on top of the pile, with a steel plate placed between the pile and the hinge to ensure a uniformly distributed load on the pile. Given the slenderness of the specimens, which might have led to buckling of the pile at low load levels, the segments were subjected to a maximum load of 80 kN, applied at load steps of 10 kN which were kept for 5 minutes. The DFOS strain readings were recorded approximately every 2 minutes, while the applied load and linear potentiometers data were recorded every second.

3.3.2. Validation of the DFOS

The main goal of mechanically testing the pile tip segments was to validate the accuracy of the DFOS strain measurements on wooden piles without influence of the soil. In order to do so, the DFOS strain readings were compared to the strain readings collected by the linear potentiometers. The Omnisens interrogator has a spatial resolution of 255 mm, while the linear potentiometers provide an average strain measurement over one-meter segments. In order to compare the data, the measurements from the DFOS had to be averaged over the one-meter segments corresponding to the position of the linear potentiometers (approximately 4 strain measurements). Finally, as mentioned in Section 3.1.3, the DFOS data might have been subjected to an initial strain, so the strain readings were zeroed at the first load step.

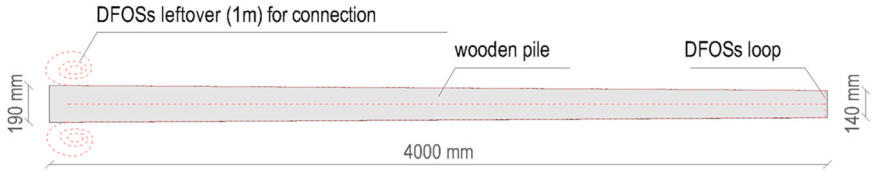

Fig. 7. DFOS set-up over the pile tip (V_V).

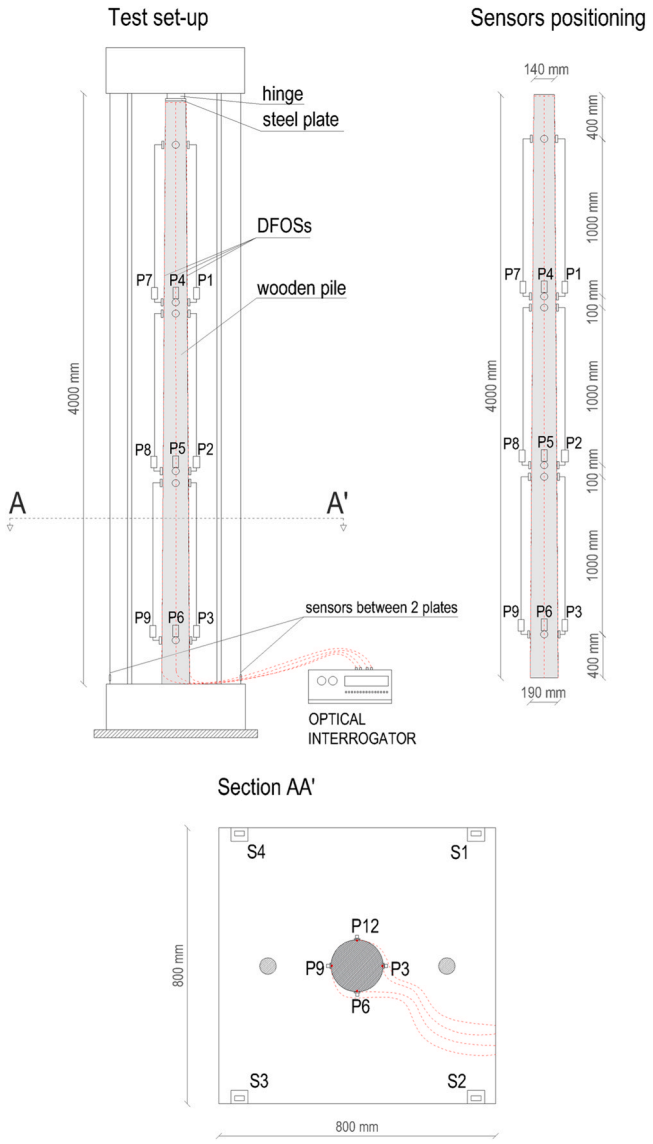

Fig. 8. Test set-up for mechanical testing of pile tips (V_V) equipped with DFOS.

4. Results

4.1. In-situ measurements

4.1.1. Cone Penetration Test (CPT)

Before pile installation in Overamstel, CPTs were conducted at each planned pile location in order to get a representative description of the soil profile. Since all piles were located at the same test site within a few meters from each other, the soil profile and cone resistance did not significantly vary for the different piles. Fig. 9 shows the soil profile collected at the location of Pile 164, together with its respective cone resistance in MPa. This soil profile will be used in the analysis (Section 5) to draw conclusions from the stress distribution acting along the length of the piles.

From Fig. 9 and Fig. 10, it can be seen that the pile head is not located at water table (NAP). The data collected by the DFOSs above water table should be disregarded, because other parameters such as temperature (direct sun exposure) and damages related to the installation of the loading set-up on the head could influence the data. The head location of each individual pile can be found in Table 1. The first soil layer (approximately 4.5 m below NAP) is a pre-drilled sand layer, which significantly influences the stress distribution in the pile given that the soil does not provide any shaft friction capacity over that length. The pre-drilled layer is followed by a peat layer of approximately 1 m and a clay layer of approximately 6 m. Finally, the second sand layer, which is the main loadbearing layer where the pile tip lays, is located at approximately −12 m NAP.

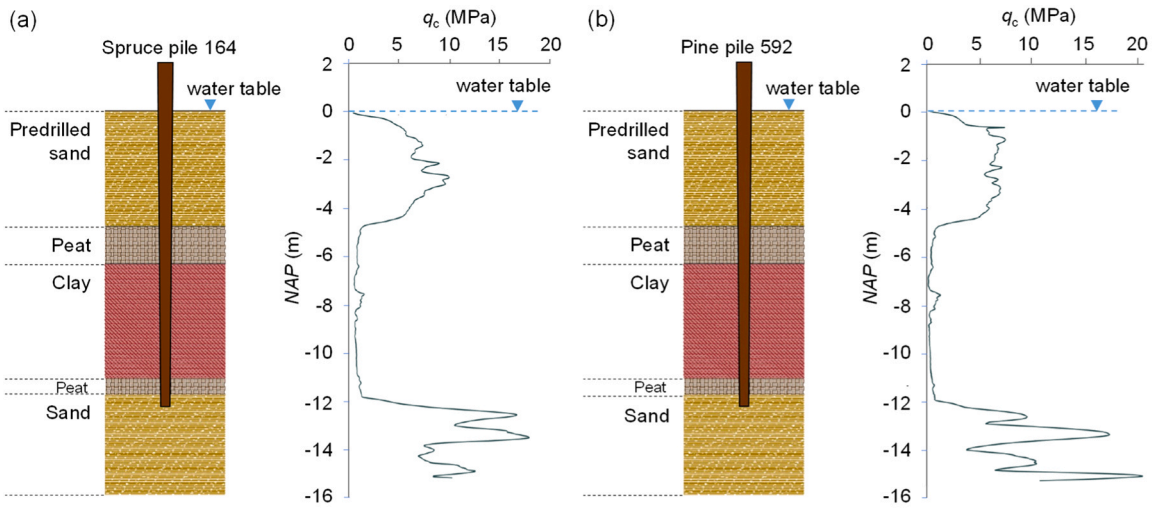

Fig. 9. Soil profile and cone resistance (q_c) for: (a) spruce pile 164; (b) pine pile 592 located in Overamstel (NL).

4.1.2. DFOS strain distribution

Each pile was tested according to the maximum load step ΔF shown in Table 1. Fig. 10 shows the strain distribution collected by the DFOS (North-South side) for Pile 164 (Fig. 10a) and Pile 576 (Fig. 10b). In the Figure, the measurements from each side of the DFOS loop can be visualized separately, the sign change is caused by the different orientation of the fiber. Each line represents the average strain measured at individual fiber locations during the specific load step timeframe. The strain measurements over both sides of the pile at each load step are symmetrical, following the expected trend based on the loading type and boundary conditions. The first 2 m of the pile, starting from the pile head, remained above the water level which corresponded to the soil level (see Fig. 9): in this part, the strains were not measured with DFOS. Fig. 11

4.2. Mechanical properties of the pile segments

The mechanical properties of 6 full-length wooden piles were characterized by determining the wet compressive strength and stiffness of 47 pile segments tested in compression. The load-displacement behaviour of the saturated spruce and pine specimens tested in compression, exhibited linearity up to 70 % - 80 % of the maximum compression load. Out of linearity, a nonlinearity phase was visible until peak load. When softening started, the load gradually decreased showing a quasi-plastic load plateau. The average mechanical properties along the length of the 3 spruce and 3 pine piles are listed in Table 3. For all piles, and relative parts, the mean wet compressive strength values are listed in Table 4.

Spruce piles exhibited an average wet compressive strength $f_{c,0,wet,mean} = 14.5$ MPa, roughly 20 % lower than pine piles, featuring $f_{c,0,wet,mean} = 18$ MPa. Comparable values of $E_{c,0,stat,wet,mean}$ were determined for both spruce and pine. The dry density ρ_{dry} (at MC = 0 %) showed a similar trend, with $\rho_{dry,mean} = 400$ kg/m^3 for spruce, 10 % lower than pine piles, where $\rho_{dry,mean} = 440$ kg/m^3 was determined.

The average mechanical properties along the pile of both spruce and pine segments are presented in the bar graphs in Figs. 12 and 13. In both spruce and pine, the wet compressive strength tended to decrease from the head to the tip of the pile, in particular in the tips, where $f_{c,0,wet,mean}$ was 20–25 % lower in relation to pile heads. Spruce and pine tip segments V-Va exhibited $f_{c,0,wet,mean} = 11 \pm 2.3$ MPa (Table 3), significantly lower than that of other tip-segments, probably because of the damage localized in this very last part due to the prior hammering of the pile. The reported strength values are related to an average dry density (MC = 0 %) for the full pile of 420 ± 30 kg/m^3. The moisture content of the pile segments, calculated before the compression test, varied along the length, ranging from 70 % to 100 %.

4.3. Strain distribution along pile tips measured with DFOS and linear potentiometers

For each pile tip, the strains were measured with DFOS along two opposite sides, and with 4 linear potentiometers (LPs) placed in sequence on each side of the pile. Figs. 13 and 14 show the DFOS and LP strain measurements under an increasing compressive load for pile 576, sides P4-P6 and P10–12 respectively. Fig. 13a and Fig. 14a show the DFOS measurements, where each dotted-line represents the average strain of a group of fibres located over the distance of a linear potentiometer (1 m). The colour coding for the position of the DFOS and LPs can be seen at the bottom of each Figure.

The pile segments are tapered, which causes small deviations on the strain level at different locations along the length. However, larger deviations could be caused by incipient buckling due to the slenderness of the segments. For pile 576, this deviation shows up after the 130 kN load step. The timber pile tips used for the DFOS validation underwent a load history consisting of driving, loading,

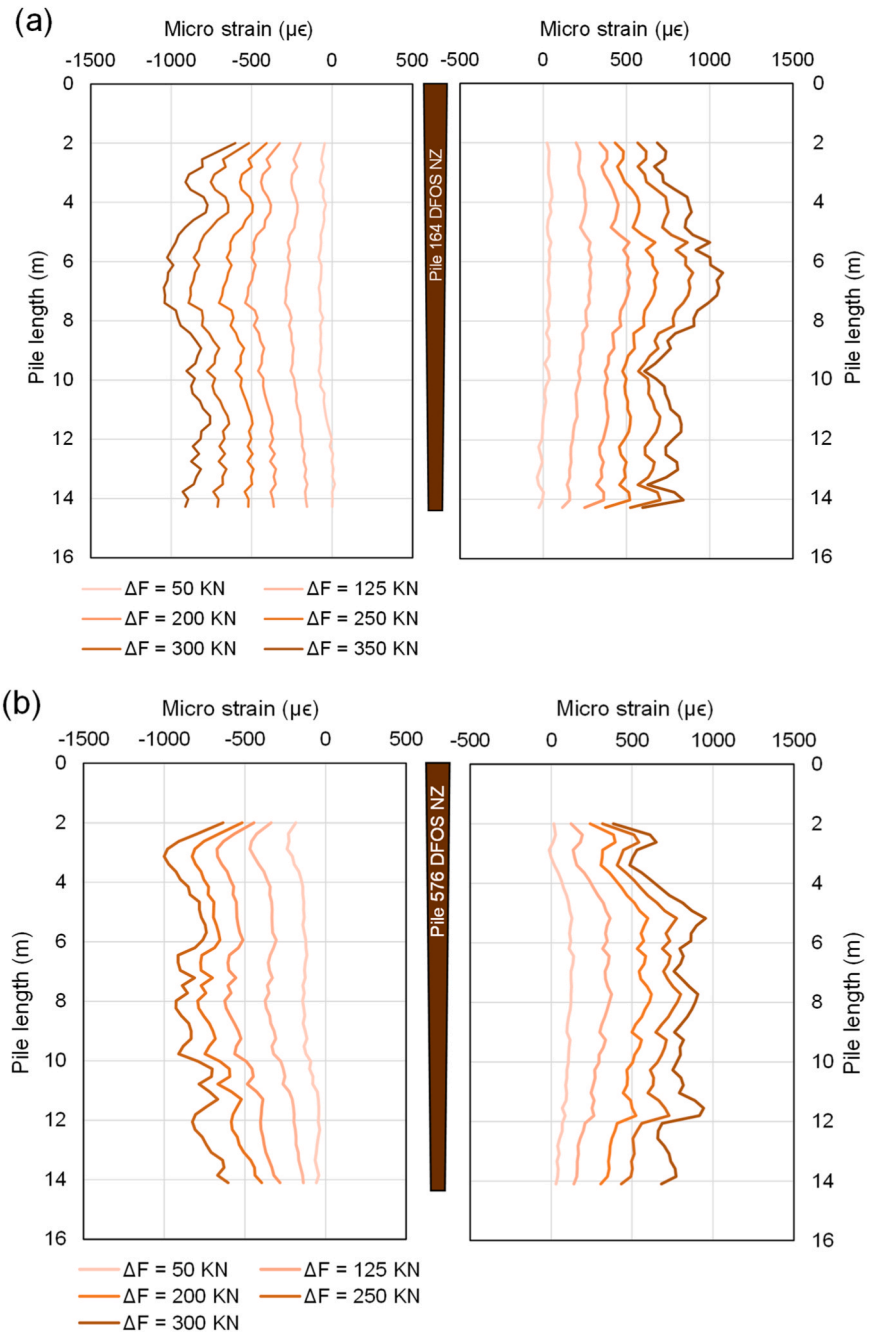

Fig. 10. In-situ strain distribution: (a) pile 164; (b) pile 576; measured with North-South DFOS, each side of the DFOS loop can be visualized separately. The y-axis represents the position of the fiber along the pile length, while the x-axis represents the strain measurement. The sign change is caused by the different orientation of the fiber.

extracting and cutting, which could potentially disturb or damage the fiber optic sensors. This was the case for the sensors (DFOS) on piles 398 and 594, which were damaged at the loop around the tip. The damage at the loop implies that only the strain readings from one side of the pile can be measured. Fig. 15 and Fig. 16 show the DFOS and LP strain readings for side P1-P3 of piles 398 and 594, respectively. Negative strains recorded by the LPs and DFOS indicate an elongation of the specimen across a specified length, attributed to the bending of the slender 4-m pile under the axial load. This can be observed in particular from the behaviour of LP3 of pile 398 (Fig. 15b) and pile 594 (Fig. 16b).

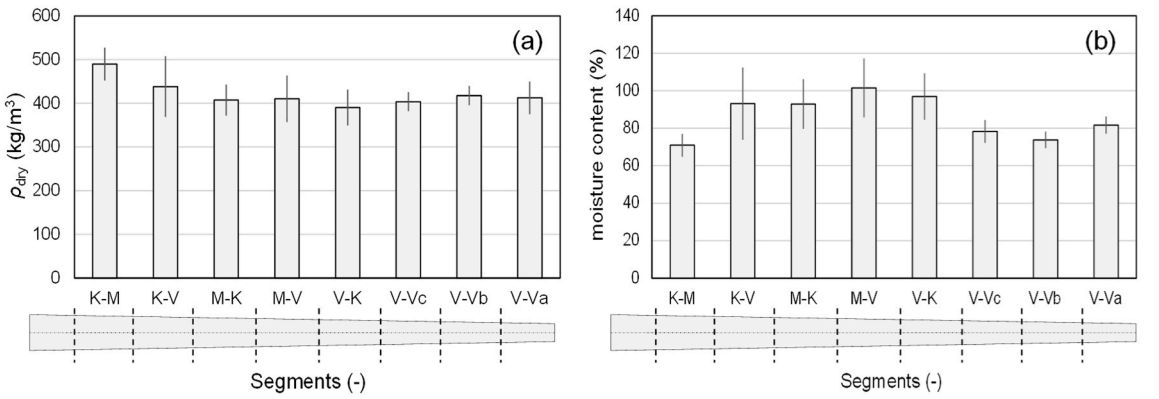

Fig. 11. (a) Average dry density (MC = 0 %); (b) average test moisture content for 47 spruce and pine segments along the pile (the vertical lines in the bar graph represent the standard deviation).

Table 3
Mechanical properties of each tested segment averaged for the 3 spruce and the 3 pine piles.

Wood species	No.	Pile part	$f_{c,0,wet}$ (MPa)		$E_{c,0,stat,wet}$ (MPa)		ρ_{wet} (kg/m^3)		ρ_{dry}[a] (kg/m^3)	
			mean	SD	mean	SD	mean	SD	mean	SD
spruce	3	K-M	16.2	1.3	11100	2730	740	84	480	51
	2	K-V	18.0	1.2	11600	930	710	36	370	24
	3	M-K	15.9	0.8	10300	1460	700	28	380	26
	3	M-V	15.0	1.2	9500	1370	700	44	360	17
	3	V-K	14.7	1.2	8900	1410	690	53	370	37
	3	V-Vc	14.1	0.5	8800	1800	630	23	390	6
	3	V-Vb	13.6	0.3	7800	860	620	23	400	20
	3	V-Va	9.8	2.3	7400	600	660	32	410	26
pine	3	K-M	20.8	1.7	11000	1130	790	64	500	35
	3	K-V	21.2	3.6	11200	1890	730	70	480	72
	3	M-K	19.4	3.1	10600	1610	710	6	430	31
	3	M-V	18.3	2.3	9500	1450	780	72	460	44
	3	V-K	17.8	3.0	9200	2360	690	40	410	54
	3	V-Vc	17.3	2.8	8400	1410	670	53	410	33
	3	V-Vb	17.3	2.2	8200	1340	690	27	430	14
	3	V-Va	11.9	1.6	7300	2380	690	78	420	58

[a] calculated at a moisture content of 0 %

Table 4
Mean wet compressive strength of different category of tested timber piles at test moisture content.

Pile part	$f_{c,0,wet}$ (MPa)	
	mean	SD
Pine + spruce full pile	16.3	3.5
Pine full pile	18.0	3.5
Spruce full pile	14.5	2.5
Pine K-M/V	21.0	2.6
Pine M-K/V	18.9	2.5
Pine V-K/Vc/Vb/Va	16.1	3.3
Spruce K-M/V	17.0	1.5
Spruce M-K/V	15.5	1.0
Spruce V-K,Vc,Vb,Va	13.0	2.3

5. Analysis

5.1. DFOS validation

The validation of the DFOS strain measurements was performed by comparing the strain measured with DFOS and the strain measurements collected by the LPs. Due to the different sampling intervals for both devices (0.25 mm for DFOS and 1 m for LPs), the

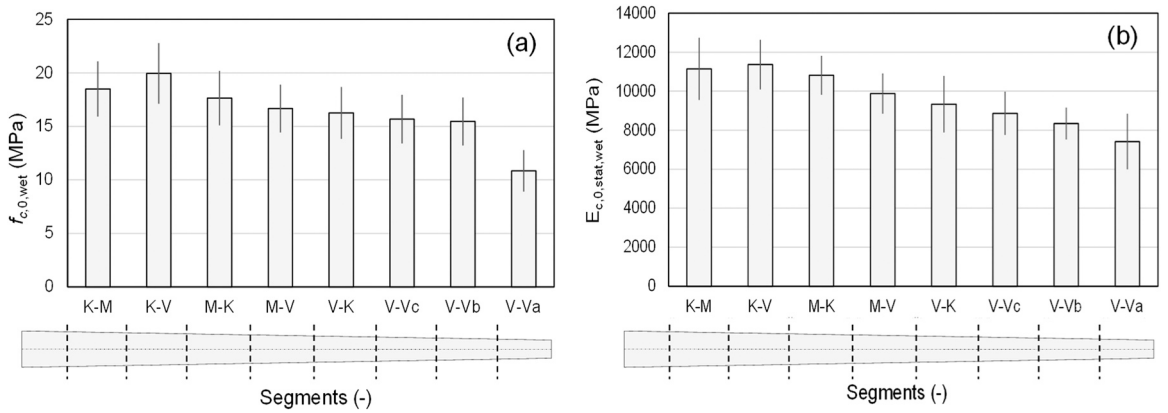

Fig. 12. (a) Average wet compressive strength $f_{c,0,wet}$; (b) average wet static modulus of elasticity $E_{c,0,stat,wet}$ for 47 spruce and pine segments along the pile (the vertical lines in the bar graph represent the standard deviation).

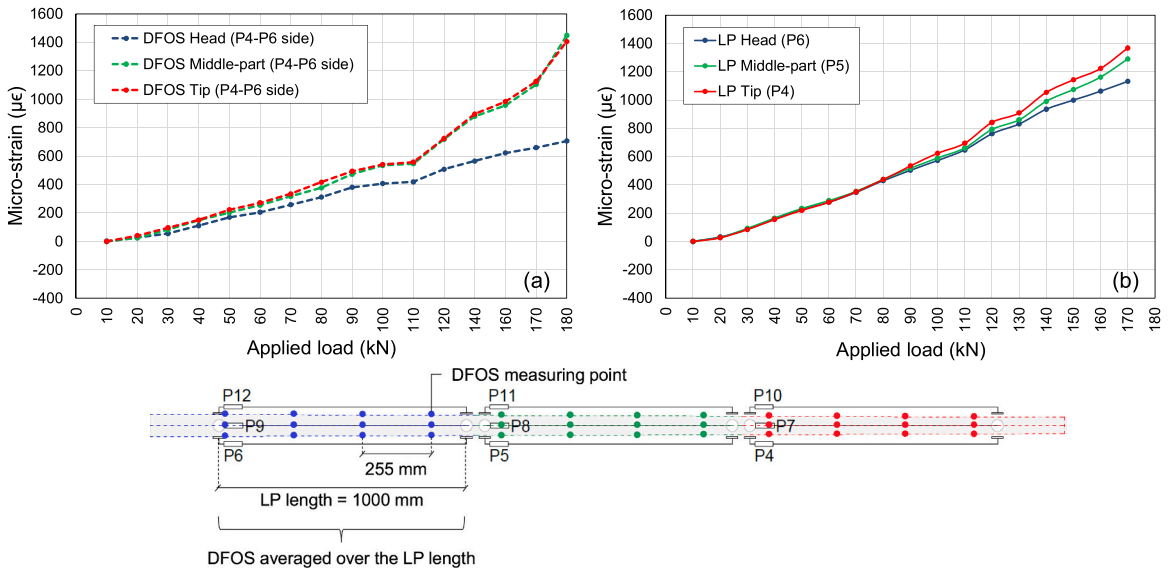

Fig. 13. Strain measurements at different load steps with (a) DFOS and (b) LPs for pile tip 576, P4-P6 side.

comparison was conducted by assessing the average strain measurements on each side of the pile. Fig. 17 shows the strain measurements for pile 576 from both the DFOS and LP over the P4-P6 and P10-P12 sides.

As previously mentioned, due to damage at the loop around the pile tips for piles 398 and 594, the DFOSs were only able to collect strain measurements over one side. Fig. 18 and Fig. 19 show the comparison between DFOS and LP strain measurements for piles 398 and 594, respectively. The deviation between the DFOS and LP measurements resulted to be significantly lower for pile 576 compared to the other two piles 398 and 594. This difference between the measurements can be explained by the accuracy level of the Omnisens interrogator. When there is a fiber loop over the specimen, the cable can be connected on both sides to the interrogator, resulting in the measuring mode BOTDA (*Brillouin Optical Time Domain Analysis*). Instead, if the loop is broken and only one end of the fiber is available, the device is set to BOTDR (*Brillouin Optical Time Domain Reflectometry*) mode. According to the technical specifications presented by the manufacturer, the BOTDA mode has a standard deviation of 7.5 με, while the BOTDR has a standard deviation of 60 με [24], which explains why pile 576 showed more accurate measurements than the other two piles. In lab condition, the less accurate BOTDR mode can result into a maximum stress deviation of $\Delta\sigma = \pm 0.65$ MPa, calculated with Eq. 3, considering the range of stiffness properties of the pile studied in this paper (see Section 4.2).

Finally, Fig. 20 shows the correlation between the DFOS and LP measurements, considering all the data collected for the 3 piles, for

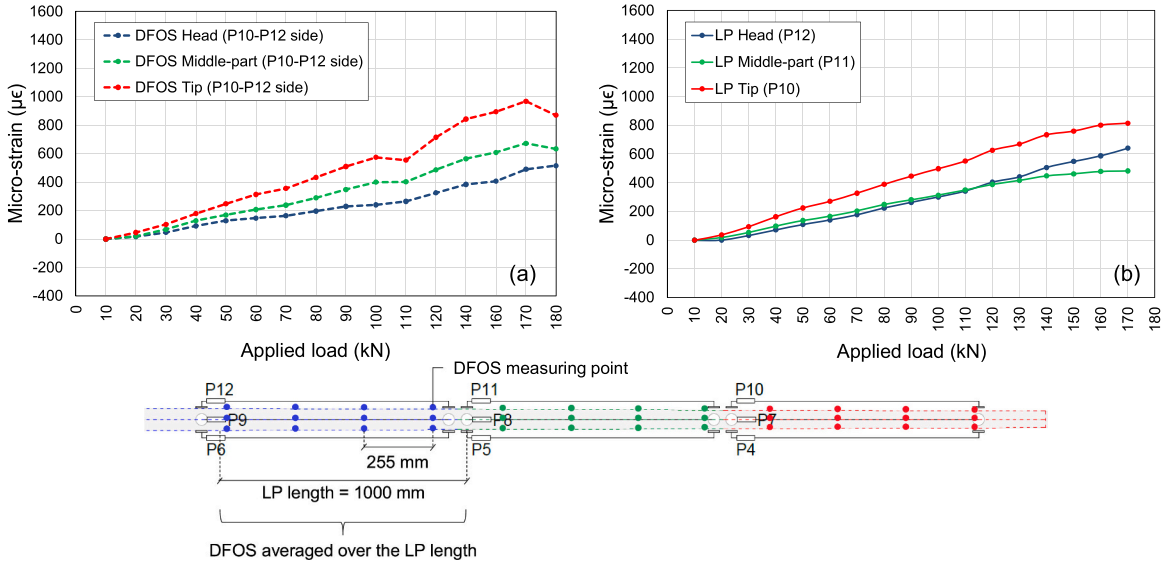

Fig. 14. Strain measurements at different load steps with (a) DFOS and (b) LPs for pile tip 576, P10-P12 side.

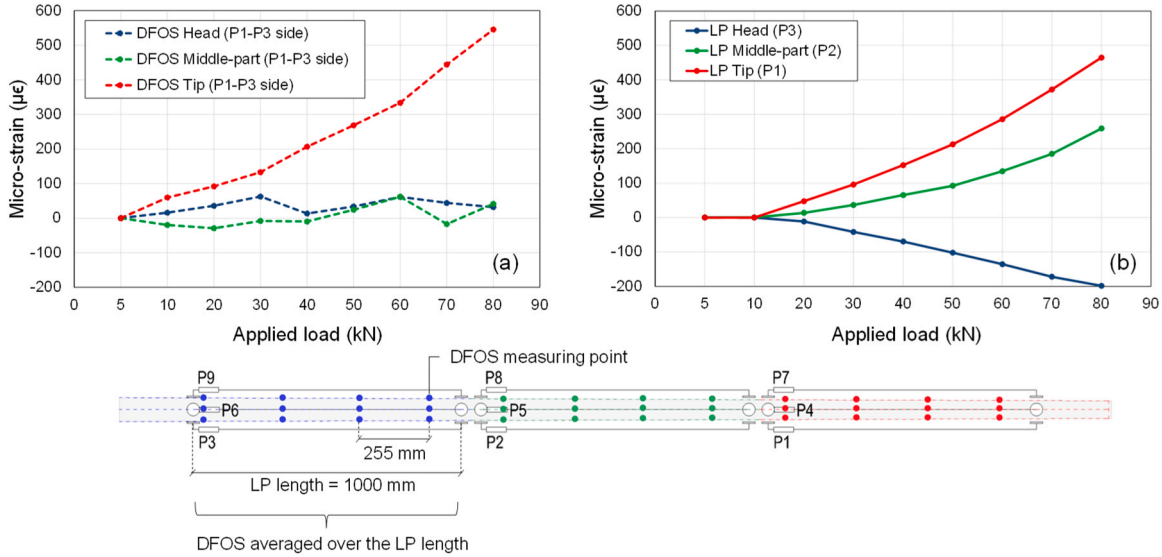

Fig. 15. Strain measurements at different load steps with (a) DFOS and (b) LPs for pile tip 398, P1-P3 side.

a total of 35 datapoints. This correlation also includes the data points exhibiting consistent behaviour related to buckling during the test. It is therefore possible to conclude that the DFOS showed an accurate estimation of the strains along the length of the specimens. However, it is important to take into account the accuracy of the mode in which the device is used. The less accurate BOTDR mode might result in larger deviations as visible for pile 594 in Fig. 20. While the BOTDA mode, used on the 4 sides of the pile 576, results in a more accurate reading also for high strain values. Considering the limited number of specimens analysed in this project, it is recommended to extend the validation to a larger sample size. This broader validation will help in establishing a scatter for better validating the accuracy of the DFOS reading.

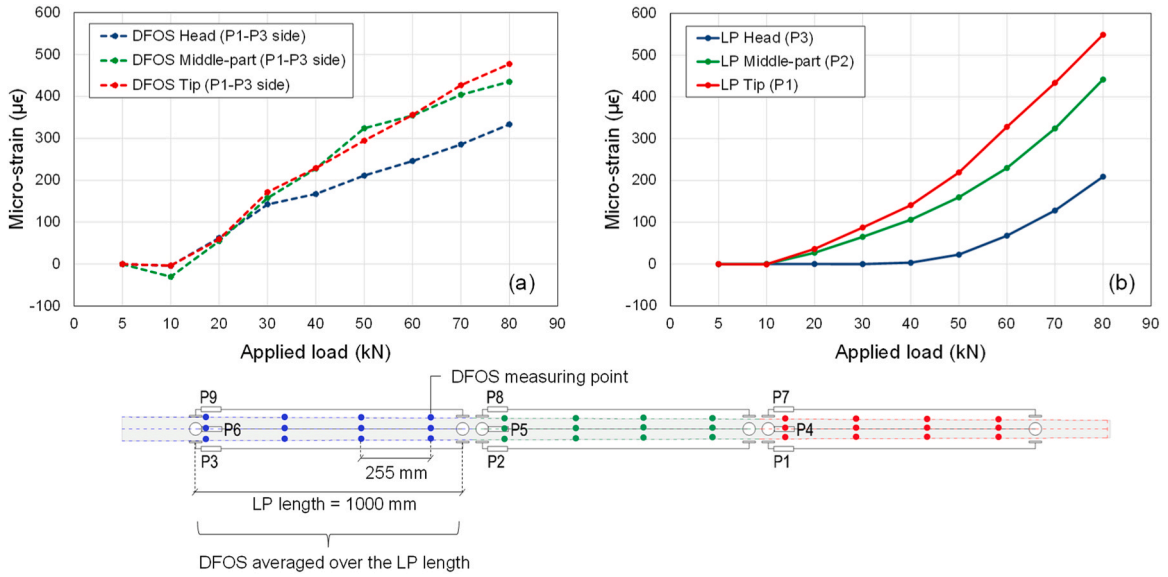

Fig. 16. Strain measurements at different load steps with (a) DFOS and (b) LPs of pile tip 594, P1-P3 side.

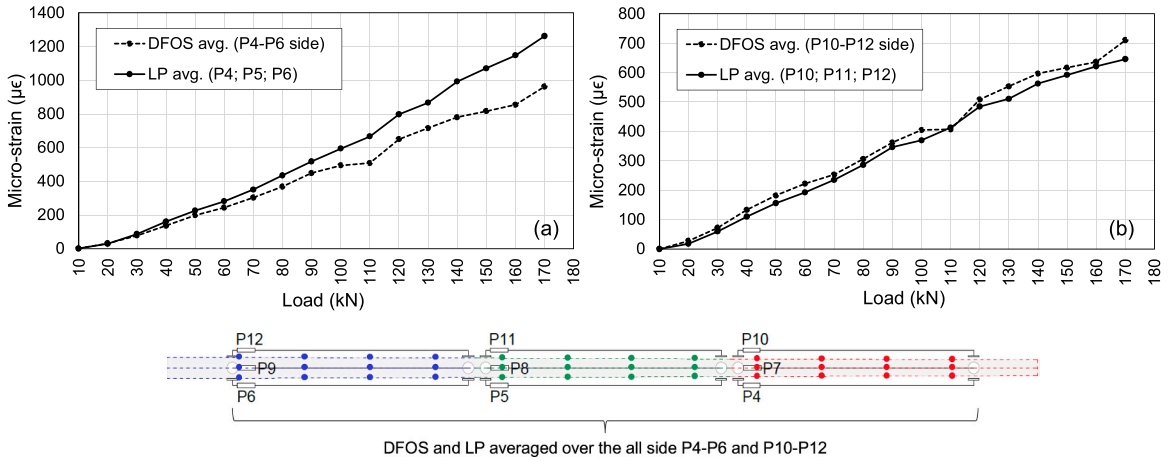

Fig. 17. Comparison between DFOS and LP strain measurements for pile tip 576, (a) P4-P6 side; (b) P10-P12 side.

5.2. *In-situ stress distribution*

The actual in-situ stress ($\Delta\sigma_{actual,stat}$) acting along the length of the piles was calculated based on Eq. 3, by using the DFOS strain readings and the static modulus of elasticity determined over the length of the pile with mechanical testing (Section 4.2). Fig. 21 shows the stress distribution over the length of pile 164 undergoing different loads steps. The y-axis presents the position of the fiber with respect to the pile head and the x-axis represents the stress in MPa. Lastly, the horizontal dashed lines represent the different soil layers, which correspond to the soil profile shown in Section 4.1. The first part of the pile (0 m - 2 m) was located above the water level which corresponded to the soil level (see Fig. 9): in this part, the strains were not measured with DFOS.

Fig. 22 shows the actual in-situ stress distribution ($\Delta\sigma_{actual,stat}$) at three different load steps compared to the no-friction stress ($\Delta\sigma_{no\text{-}friction}$) for pile 164. The no-friction stress is considered as the stress acting across the pile cross-section in the absence of shaft friction between the pile and the soil. This is based on the assumption that no shaft friction occurs between the pile and the soil, resulting in the actual stress being equal to the no-friction stress. However, at the lowest load step of $\Delta F = 50$ kN (Fig. 22a), it can be noticed that $\Delta\sigma_{actual,stat}$ over the predrilled layer is lower than $\Delta\sigma_{no\text{-}friction}$: this might be indicative of a slight, residual shaft friction between the pile and the predrilled sand layer at low mobilization displacements. After the predrilled sand layer, the pile shows a higher interaction with the soil via large deviations between the actual and no-friction stress distributions. At the load step $\Delta F = 200$ kN (Fig. 22b) the actual and no-friction stress distributions follow the expected behaviour, where both graphs overlap within the predrilled sand layer, and start to deviate right at the boundary of the soil layer. At the maximum load level $\Delta F = 350$ kN (Fig. 22c), a very similar behaviour

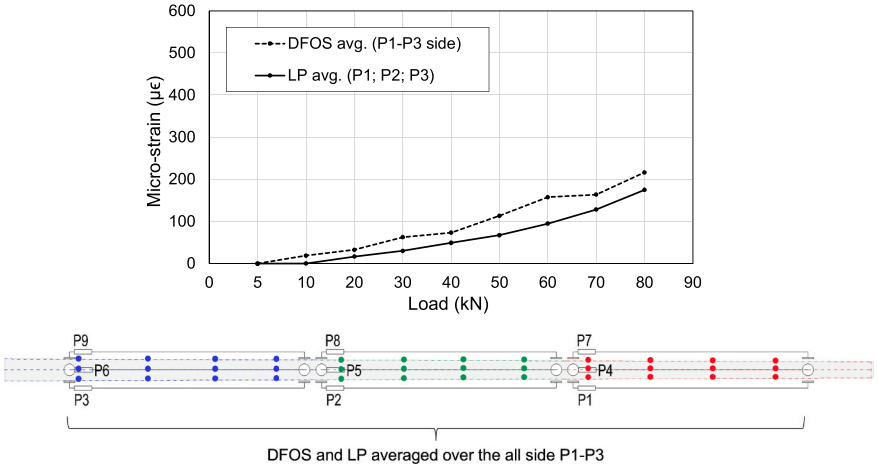

Fig. 18. Comparison between DFOS and LP strain measurements for pile tip for pile 398, side P1-P3.

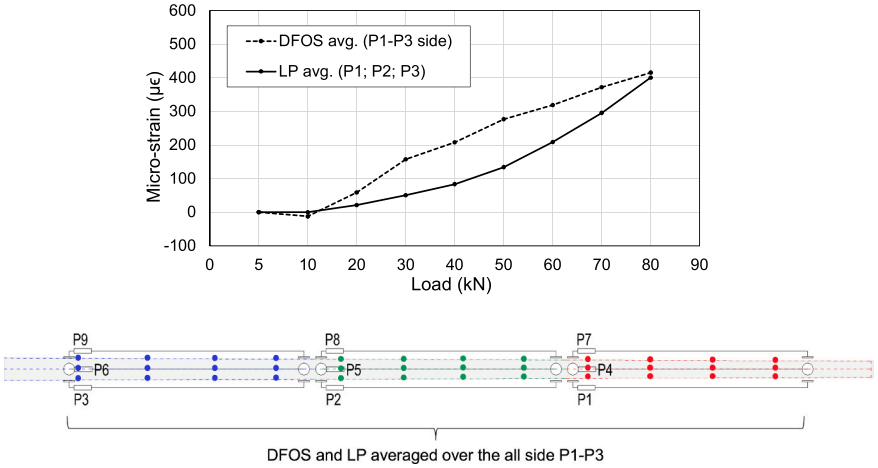

Fig. 19. Comparison between DFOS and LP strain measurements for pile 594, side P1-P3.

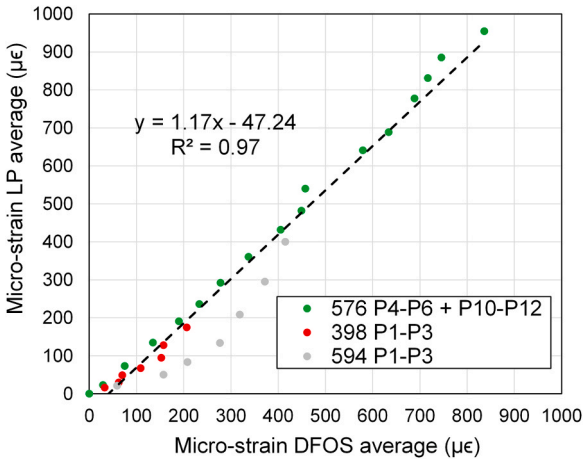

Fig. 20. Correlation between strains measured with DFOS and LPs, including 35 datapoints from pile 576, 398 and 594.

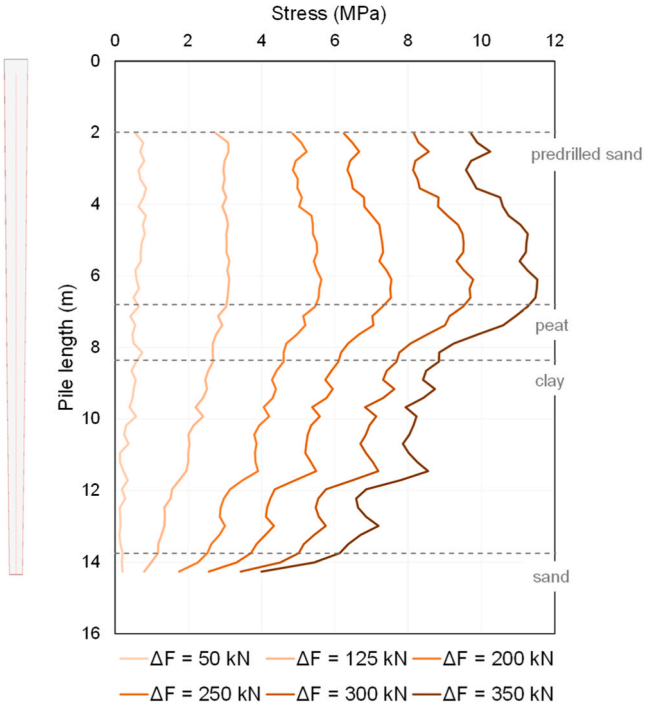

Fig. 21. In-situ stress distribution of pile 164 undergoing 6 different load steps.

is observed; however, within the pre-drilled sand layer, the actual stress distribution is slightly higher than the no-friction stress. This deviation, reaching a maximum of 1.8 MPa, is caused by the standard deviation of the DFOS measurements discussed in Section 5.1, and possibly by other uncertainties given by the in-situ set-up.

Additionally, the distribution of $\Delta\sigma_{actual,stat}$ and $\Delta\sigma_{no\text{-}friction}$ at the maximum load step are shown for piles 576 (Fig. 23a), 594 (Fig. 23b), 398 (Fig. 23c), 397 (Fig. 23d) and 592 (Fig. 23e). It can be observed that the distribution of the stresses over the predrilled sand layer corresponds to the expected behaviour where the actual and the no-friction stresses overlap, with a deviation within 2 MPa. For pile 576 (Fig. 23a), it can be noticed that the deviation between the stresses starts before the boundary of the predrilled sand layer, which highlights the presence of shaft friction after the predrilled layer.

As explained in Section 3.1.1, During in-situ testing, the highest load step corresponded to the geotechnical failure of the pile, which did not correspond to the material failure. This can be observed in Fig. 22 and Fig. 23, where $\Delta\sigma_{actual,stat}$ reached during in-situ testing was always below the compressive strength of the material (See Table 4).

Finally, Fig. 24 shows the in-situ stress distribution at maximum load level (350 kN) for spruce pile 164 and pine pile 592, when calculated both with the distribution of $E_{c,0,stat,wet}$ of each tested segment, described in Section 4.2, and with $E_{c,0,dyn,wet}$ for the whole pile. The wet compressive strength distribution ($f_{c,0,wet}$) determined with mechanical testing for each segment is also presented along pile 164 (Fig. 24a) and 592 (Fig. 24b). The in-situ stress distribution $\Delta\sigma_{actual,dyn}$ calculated with the dynamic modulus of elasticity of the pile could lead to an overestimation of the stresses of up to 3 MPa in the critical section of the pile, which can become governing when assessing its load bearing capacity. In each in-situ test, $\Delta\sigma_{actual,dyn}$ remained below the compressive strength $f_{c,0,wet}$. This can be attributed to the presence of shaft friction between the pile and the soil. Without this frictional resistance, the pile stresses would have exceeded the compressive strength.

6. Conclusions and recommendations

The study presented in this paper aimed to evaluate the actual in-situ stress distribution acting along the length of 3 spruce (*Picea abies*) and 3 pine (*Pinus sylvestris*) foundation piles axially loaded into the soil. The in-situ stress distribution $\Delta\sigma_{actual,stat}$ was determined by using DFOS strain measurements and the distribution of the static stiffness properties of the piles ($E_{c,0,stat,wet}$), which were determined with mechanical testing on pile segments. The method needed to be validated due to its novel and limited application on timber

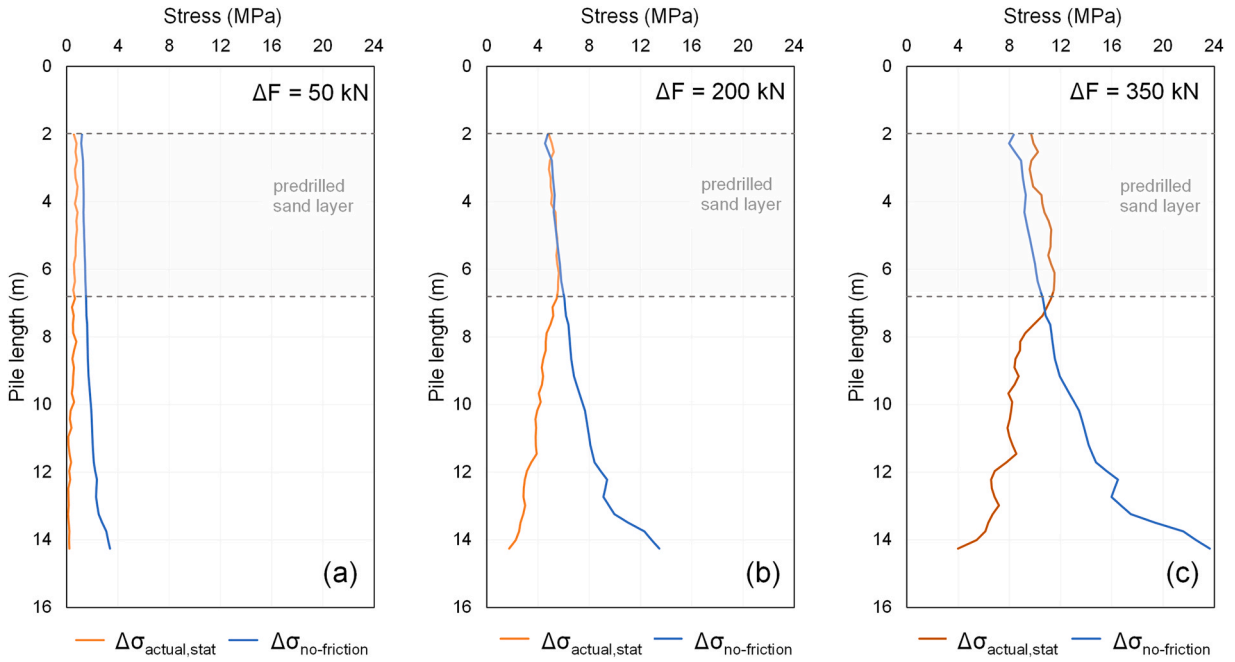

Fig. 22. In-situ stress distribution of pile 164 at load steps (a) ΔF = 50 kN; (b) ΔF = 200 kN; (c) ΔF = 350 kN.

foundation piles.

On the basis of axial compression tests conducted in the laboratory on 4-m pile tip segments equipped with DFOS and LP, the DFOS strain measurements were validated by comparing the output from both devices. The DFOS output showed a high correlation with that from the LPs, confirming that the DFOSs can be applied to axially loaded timber foundation piles. During the measurements, it was found that the accuracy of the DFOSs is related to the interrogator mode used while collecting the data. When both ends of the cable are connected to the interrogator, this provides results with higher accuracy, due to an inherited low standard deviation SD = 7.5 με (BOTDA mode). Instead, when only one end of the cable is connected to the interrogator, the accuracy is lower, with SD = 60 με (BOTDR mode).

In the application of DFOS to in-situ timber foundation piles, the initial strains recorded in the DFOS readings, attributed to the installation process, were zeroed in order to accurately assess the stress distribution along the length of the pile induced by the applied in-situ loading protocol. It should be noted that the DFOSs were glued to the outer part of the pile and thus might have been exposed to external damage, with a consequent possible interruption of the signal in correspondence to the damage position. In case of damage, the BOTDA mode would not be applicable, leading to the use of BOTDR mode with higher standard deviation, and resulting in lower accuracy of the strain measurement. Therefore, it is recommended to glue the DFOSs more internally on the side of the pile to minimize the possibility of damage during pile driving.

From the mechanical testing of the pile segments, the wet compressive strength and stiffness values parallel to the grain ($f_{c,0,wet}$ and $E_{c,0,stat,wet}$), the wet density (ρ_{wet}) along the length of each pile were determined, for a moisture content higher than 70 %. A wet mean compressive strength value of $f_{c,0,wet,mean} = 14.5 \pm 2.5$ MPa was derived for spruce and $f_{c,0,wet,mean} = 18.0 \pm 3.5$ MPa for pine, for the whole piles. In both spruce and pine, the wet compressive strength was decreasing from the head to the tip of the pile, in particular in the tips, where $f_{c,0,wet,mean}$ appeared to be roughly 20–25 % lower in relation to pile heads.

Using the wet static modulus of elasticity of the piles collected in the laboratory and the in-situ DFOS strain measurements, it was possible to determine the actual in-situ stress distribution acting along the piles while subjected to compressive loads. Based on the assumption that the mobilized pile has no shaft friction over the region of the predrilled sand layer, it was possible to compare the measured stress $\Delta\sigma_{actual,stat}$ with the no-friction stress $\Delta\sigma_{no\text{-}friction}$. It was found that $\Delta\sigma_{actual,stat}$ over the predrilled layer, corresponded to the expected $\Delta\sigma_{no\text{-}friction}$ with a maximum deviation of up to 2 MPa, which could be caused by the interaction with the soil, given the external application of the DFOS. Further into the soil, after the predrilled layer, the stress distribution followed the expected behaviour, decreasing over the length of the pile due to the shaft capacity and variation in mechanical properties. At the tip level, it was observed that the in-situ actual stresses $\Delta\sigma_{actual,stat}$ at the maximum load step (ΔF = 300–375 kN) ranged at 4 – 7 MPa, while the no-friction stresses $\Delta\sigma_{no\text{-}friction}$ ranged at 20 – 26 MPa, highlighting the effect of the shaft capacity. Additionally, the in-situ stress distribution $\Delta\sigma_{actual,dyn}$ was assessed considering a single value of wet dynamic modulus of elasticity of the pile ($E_{c,0,dyn,wet}$): this led to an

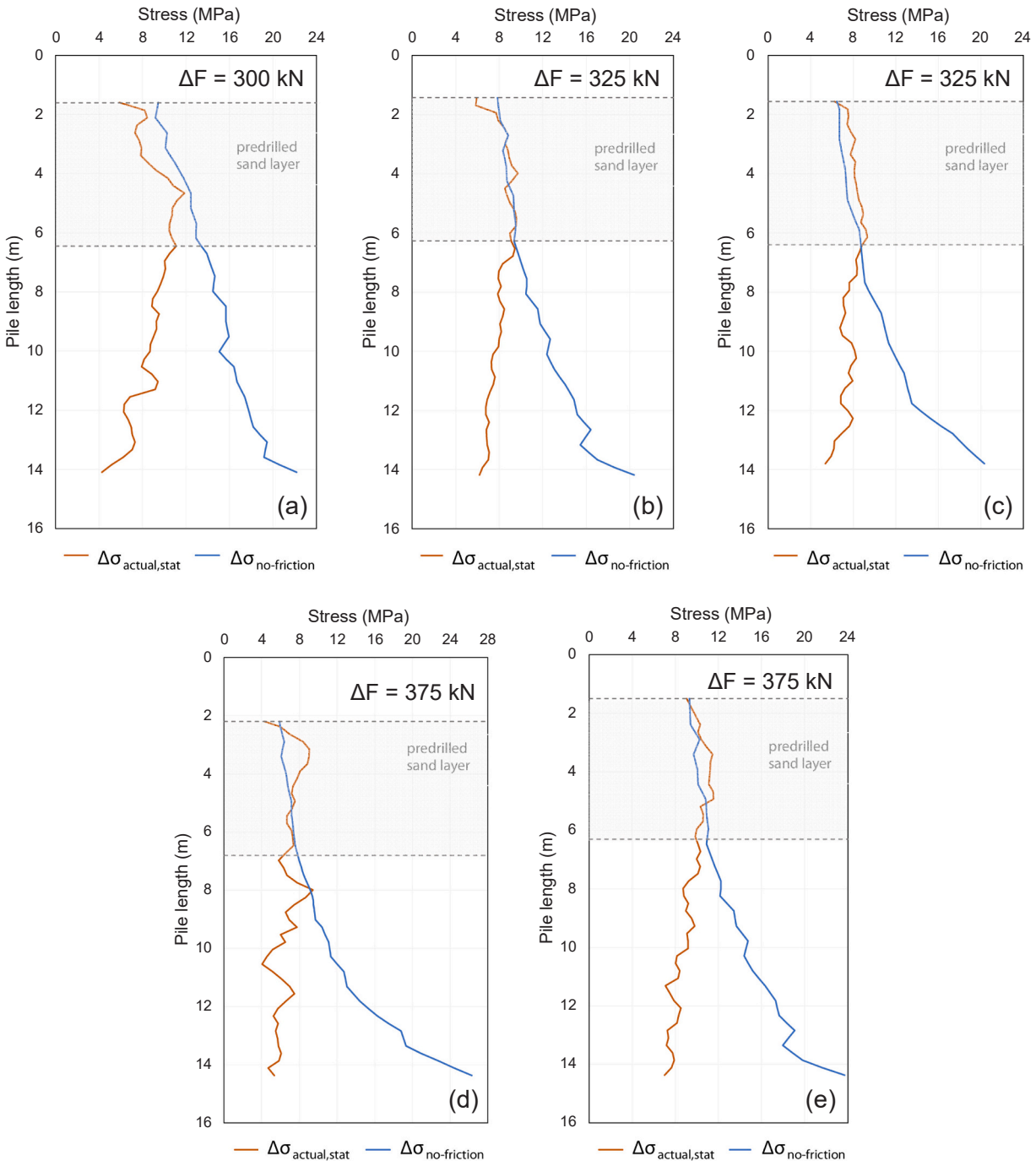

Fig. 23. In-situ stress distribution at maximum load step of piles (a) 576; (b) 594; (c) 398; (d) 397; (e) 592.

overestimation of the stresses at tip level of approximately 3 MPa, which based on the measured compression strength properties could become governing in the assessment of the piles. In the in-situ test, both $\Delta\sigma_{actual,stat}$ and $\Delta\sigma_{actual,dyn}$ remained below the compressive strength $f_{c,0,wet}$ of the pile. This can be attributed to the presence of shaft friction between the pile and the soil. Without this frictional resistance, the pile stresses would have exceeded the compressive strength.

The accuracy of the DFOS used for axially loaded piles in the laboratory was assessed with a maximum deviation of 0.65 MPa. However, in the in-situ tests, the quality of the readings varied compared to the controlled lab conditions, resulting in a deviation up to 2 MPa. This discrepancy could be attributed to external factors, including possible in-situ damage of the DFOSs, glued to the external part of the pile, and other uncertainties arising from the in-situ setup.

The findings of this case study underscore the variability in the mechanical properties along the length of timber piles, emphasizing

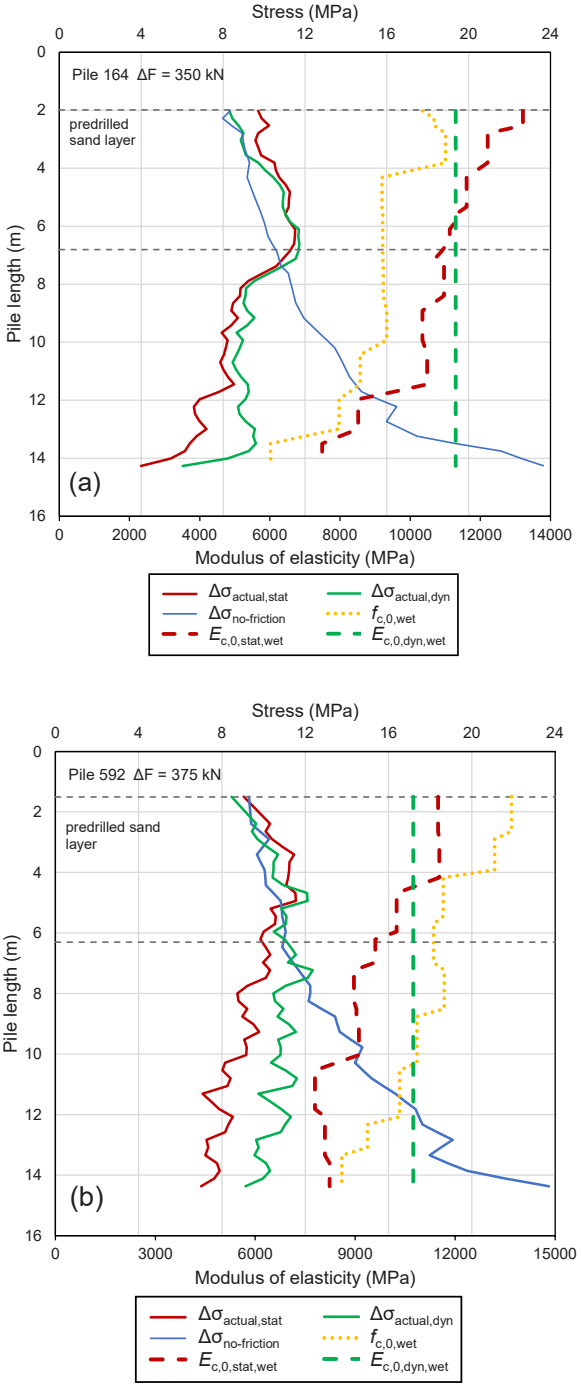

Fig. 24. In-situ stress distribution at maximum load step and mechanical properties of (a) spruce pile 164; (b) pine pile 592.

the importance of considering specific geometrical and mechanical properties when assessing the stress distribution within a timber foundation pile and its interaction with the soil. Moreover, the study highlights the potential of using DFOS for investigating the behaviour of in-situ timber piles. This opens up the opportunity for the improvement and revision of analytical methods currently adopted for the estimation and monitoring of the load carrying capacity of wooden foundations piles.

CRediT authorship contribution statement

Geert Ravenshorst: Writing – review & editing, Supervision, Project administration, Funding acquisition. **Giorgio Pagella:** Writing – review & editing, Writing – original draft, Visualization, Project administration, Methodology, Investigation, Formal analysis, Data curation, Conceptualization. **Jan-Willem van de Kuilen:** Resources, Project administration, Funding acquisition. **Michele Mirra:** Writing – review & editing, Validation, Supervision. **Maria Felicita:** Writing – review & editing, Writing – original draft, Methodology, Investigation, Formal analysis, Data curation, Conceptualization.

Declaration of Competing Interest

The authors declare the following financial interests/personal relationships which may be considered as potential competing interests: Biobased structures and materials group-TU DELFT reports equipment, drugs, or supplies was provided by Municipality of Amsterdam. If there are other authors, they declare that they have no known competing financial interests or personal relationships that could have appeared to influence the work reported in this paper.

Data Availability

The data that has been used is confidential.

Acknowledgements

The Authors gratefully acknowledge the Municipality of Amsterdam for having funded the research study and provided the analysed wooden foundation piles, along with the Municipality of Rotterdam and Deltares (The Netherlands), for having conducted the readings of the DFOS of the piles. A final acknowledgement to Ruben Kunz, for his help in performing the experimental tests.

References

[1] R.K.W.M. Klaassen, J.G.M. Creemers, Wooden foundation piles and its underestimated relevance for cultural heritage, Supplement, 2012, Pages S123-S128, ISSN 1296-2074, J. Cult. Herit. Volume 13 (Issue 3) (2012), https://doi.org/10.1016/j.culher.2012.02.014.
[2] R.K.W.M. Klaassen, Bacterial decay in wooden foundation piles—Patterns and causes: a study of historical pile foundations in the Netherlands, 2008, Pages 45-60, ISSN 0964-8305,, Int. Biodeterior. Biodegrad. Volume 61 (Issue 1) (2008), https://doi.org/10.1016/j.ibiod.2007.07.006.
[3] J. Elam, C. Björdal, A review and case studies of factors affecting the stability of wooden foundation piles in urban environments exposed to construction work, 2020, 104913, ISSN 0964-8305, Int. Biodeterior. Biodegrad. Volume 148 (2020), https://doi.org/10.1016/j.ibiod.2020.104913.
[4] J.W.G. Van de Kuilen, Service life modelling of timber structures, 2007, Mater. Struct. 40 (1) (2007) 151–161, https://doi.org/10.1617/s11527-006-9158-0.
[5] Van de Kuilen, J.W.G., Beketova-Hummel, O., Pagella, G., Ravenshorst, G.J.P., Gard., W. (2021). An integral approach for the assessment of timber pile foundations. In: World Conference on Timber Engineering 2021, WCTE 2021, pp. 2–8, Santiago, Chile, 2021.
[6] Mirra, M., Pagella, G., Gard, W.F., Ravenshorst, G.J.P., van de Kuilen, J.W.G. (2023). Influence of moisture content on the assessment of decay levels by micro-drilling measurements in wooden foundation piles. World Conference on Timber Engineering, Oslo, Norway, 2023.
[7] M. Mirra, G. Pagella, M. Lee, W. Gard, G. Ravenshorst, J.W.G. Van de Kuilen, Characterisation of bacterial decay effects on wooden foundation piles across various historical periods, 2024, 135670, ISSN 0950-0618, Constr. Build. Mater. Volume 421 (2024), https://doi.org/10.1016/j.conbuildmat.2024.135670.
[8] Pagella, G., Ravenshorst, G.J.P., Gard, W., van de Kuilen, J.W.G. (2022). Characterization and assessment of the mechanical properties of spruce foundation piles retrieved from bridges in Amsterdam. International Conference on Timber Bridges ICTB2021plus, Biel, Switzerland, 2022. ⟨https://doi.org/10.24451/cmes-1s31⟩.
[9] EN 1995–1-1 (2010)+AC (2006)+A1 (2008) Eurocode 5: design of timber structures–part 1–1: General–common rules and rules. European Committee for Standardization (CEN), Brussels, Belgium (2010).
[10] NEN-EN 1995–1-1/NB:2013. Dutch National annex to NEN-EN 1995–1-1. Eurocode 5: design of timber structures–part 1–1: General–common rules and rules for buildings (includes C1+A1/C1:2012). Netherlands Standardisation Institute (NEN), Delft, The Netherlands (2013).
[11] NEN 5491:2010. Quality requirements for wood (KVH 2010) - Piles - European softwood. Netherlands Standardisation Institute (NEN), Delft, The Netherlands (2010) (in Dutch).
[12] NEN-EN 1995–1-1/NB:2007. Dutch National annex to NEN-EN 1995–1-1. Eurocode 5: design of timber structures–part 1–1: General–common rules and rules for buildings (includes C1:2006). Netherlands Standardisation Institute (NEN), Delft, The Netherlands (2007).
[13] G. Pagella, M. Mirra, G.J.P. Ravenshorst, J.W.G. Van de Kuilen, Influence of knots and density distribution on compressive strength of wooden foundation piles. In Current Perspectives and New Directions in Mechanics, Current Perspectives and New Directions in Mechanics, Modelling and Design of Structural Systems (2022) 2022.
[14] J. Malinen, M. Maltamo, E. Verkasalo, Stem and wood properties of norway spruce on drained peatlands and mineral forest lands in Southern Finland, Balt. For. 11 (2005) 21–38.
[15] G. Riesco Muñoz, M.A. Soilán Cañas, R. Roíguez Soalleiro, Physical properties of wood in thinned Scots pines (Pinus sylvestris L.) from plantations in northern Spain, Ann. . Sci. 65 (2008) (2008) 507, https://doi.org/10.1051/forest:2008026.
[16] J.C.F. Walker. Primary Wood Processing: Principles and Practice, 2nd edn., Springer, Dordrecht, 2006, p. 596.
[17] Draft prEN 1995-1-1 (2023). New Eurocode 5: Design of timber structures — common rules and rules for buildings — part 1-1: General. Netherlands Standardisation Institute (NEN), Delft, The Netherlands (2023).
[18] NEN 9997-1/C2:2017. Geotechnical design of structures - part 1: general rules, Netherlands Standardisation Institute (NEN), Delft, The Netherlands (2017) (in Dutch).
[19] NEN 6760:1997 (NL). Technische grondslagen voor bouwconstructies - TGB 1990 - Houtconstructies - Basiseisen en bepalingsmethoden (in Dutch) Netherlands Standardisation Institute (NEN), Delft, The Netherlands (1997)

[20] N. De Battista, C. Kechavarzi, H. Seo, H. Soga, S. Pennington, Distributed fibre optic sensors for measuring strain and temperature of cast-in-situ concrete test piles. Proceedings of the International Conference on Smart Infrastructure and Construction (ICSIC), ICE Publishing, London, 2016, p. 2016.
[21] A. Klar, P.J. Bennett, K. Soga, R.J. Mair, P. Tester, R. Fernie, H.D. St John, G. Torp-Peterson, Distributed strain measurement for pile foundations, Proc. Inst. Civ. Eng. - Geotech. Eng. 2006 159 (3) (2006) 135–144.
[22] C. Kechavarzi, L. Pelecanos, N. De Battista, K. Soga, Distributed fibre optic sensing for monitoring reinforced concrete piles, Geotech. Eng. 50 (2019) 43–51.
[23] Fujikura Ltd. (2012). Optical Fiber Indoor Cable with Low Friction (LF) coating. ⟨http://fujikura.su/en/production/ftth/optical-low-friction-cable.html⟩. Last visited 6.2.2024.
[24] ⟨https://www.omnisens.com/⟩ last visited 18.09.2023.
[25] Fidanboylu, K. (2009). Fiber optic sensors and their applications. International Advanced Technologies Symposium (IATS'09).
[26] EN 384:2016+A2:2022. Structural timber–Determination of characteristic values of mechanical properties and density. European Committee for Standardization (CEN), Brussels, Belgium (2016)
[27] NEN-EN 13183-1:2002. Moisture content of a piece of sawn timber - Part 1: Determination by oven dry method. Netherlands Standardisation Institute (NEN), Delft, The Netherlands (2002).
[28] EN 408 (2010)+A1 (2012). Timber structures–structural timber and glued laminated timber–determination of some physical and mechanical properties. European Committee for Standardization (CEN), Brussels, Belgium (2010).
[29] EN 14251 (2003). Structural round timber - Test methods, European Committee for Standardization (CEN), Brussels, Belgium (2003).
[30] Ravenshorst, G.J.P., Van de Kuilen, J.W.G. (2009). Relationships between local, global and dynamic modulus of elasticity for soft- and hardwoods. CIB W18, proceedings paper 42-10-1, Dubendorf, Switzerland, 2009.